Super hard cubic phases of period VI transition metal nitrides: First principles investigation

S.K.R. Patil [a], N.S. Mangale [b], S.V. Khare [c,*], S. Marsillac [c]

[a] Department of Mechanical Engineering, The University of Toledo, Toledo, OH 43606, USA
[b] Department of Electrical Engineering and Computer Science, The University of Toledo, Toledo, OH 43606, USA
[c] Department of Physics and Astronomy, The University of Toledo, 2801 West Bancroft Street, Toledo, OH 43606, USA

ABSTRACT

We report a systematic study of mechanical and electronic properties of 32 cubic phases of nitrides of the transition metals M (M = Hf, Ta, W, Re, Os, Ir, Pt, Au), in zinc-blende, rocksalt, pyrite, and fluorite structure using *ab initio* computations. Our results reveal that MN_2 (M = W, Re, Os, Ir, Pt, Au) in pyrite phase, have a bulk moduli greater than 330 GPa, MN_2 (M = Re, Os, Ir) in fluorite phase have a bulk moduli greater than 350 GPa and TaN in rocksalt phase has a bulk modulus of 380 GPa making them candidates for super hardness. Based on the bulk and shear modulus for stable phases, potential hard coating materials for cutting tools have been identified. The local density of states of all phases has been obtained and linked to mechanical stability. The high values of bulk moduli are attributed to strong bonding of transition metal d-orbitals with nitrogen p-orbitals. The trend in the bulk modulus is related to the valence electron density of these materials.

© 2008 Elsevier B.V. All rights reserved.

1. Introduction

Hard coatings of many transition metal nitrides have ubiquitous applications in manufacturing and semiconductor industries because of their extreme hardness, wear and corrosion resistance, and suitable thermal and electrical properties [1–4]. Discovery of the nitrides of the noble metals Au and Pt has been wanting till recently [5,6]. Synthesis of super hard platinum nitride by Gregoryanz et al. [6] and Crowhurst et al. [7] using laser heated diamond anvil cells has paved the way for the discovery of other potential hard transition metal nitrides (TMNs). Subsequently [7,8] IrN_2 and OsN_2 with a high bulk modulus (*B*) of 428 GPa, second only to diamond, and 358 GPa respectively, have also been experimentally synthesized. Recent *ab initio* investigations [9,10] predicted IrN_2 and OsN_2 to be hard which was later confirmed by the experiments [7,8]. These studies [5–10] have led to the question: Do other hard TMNs exist and if so, do they possess hardness? Motivated by this question and the potential applications of these TMNs in the hard coatings industry, we have begun a systematic quest to find super hard TMNs using first principle calculations which are reported in this letter.

Many transition metal nitrides exist in zinc-blende and rocksalt structure. Experiments of Gregoryanz et al. [6] reported that PtN, the first noble TMN to be synthesized, was also a zinc-blende structure. Later theoretical investigations [11–13] showed that zinc-blende structure was mechanically unstable and the synthesized PtN was not zinc-blende. Yu and Zhang [13] then proposed that the

synthesized compound was fluorite PtN_2 as it yielded a value of bulk modulus (B) closer to the experimental value. Subsequently it was proved [8,14] that the crystal structure was pyrite. IrN_2 and OsN_2 in fluorite phase were found to have a high *B* of 381 GPa [9] and 367 GPa [10] respectively using *ab initio* calculations. Recent theoretical studies [15,16] proposed marcasite phase for the synthesized OsN_2. In spite of active theoretical and experimental research, only the structure of PtN_2 is known to be pyrite. The crystal structure of synthesized IrN_2 and OsN_2 is yet to be determined [16]. Motivated by this background we have theoretically studied the cubic phases: zinc-blende, rocksalt, fluorite, and pyrite with a goal of finding candidate materials for hard coating applications.

2. Computational method

We performed *ab initio* total energy calculations within the local density approximation (LDA) to density functional theory [17] using the suit of codes VASP [18–21]. Core electrons are implicitly treated by ultrasoft Vanderbilt type pseudo potentials [22] as supplied by Kresse and Hafner [23]. For each calculation, irreducible *k*-points are generated according to the Monkhorst–Pack scheme [24]. The single-particle wave functions have been expanded in a plane-wave basis using a 300 eV kinetic energy cutoff. All atoms are allowed to relax until a force tolerance of 0.001 eV/Å is reached for each atom. The calculations for the local density of states (DOS) were performed with the tetrahedron method with Blöchl [25] corrections for the energy. Tests using a higher plane-wave cutoff and a larger *k*-point sampling indicate that a numerical convergence better than ± 1.0 meV is achieved for relative energies.

* Corresponding author. Tel.: +1 419 530 2292.
  E-mail address: khare@physics.utoledo.edu (S.V. Khare).

To obtain the absolute minimum in total energy for each crystal structure, the lattice constant (a) and the internal degree of freedom u (for pyrite phase) were varied independently. The obtained total energies were fit to the equation of Teter et al. [26] to obtain the equilibrium lattice constant and B. Once the equilibrium constants and volume were established for each structure, external strains δ of ±1%, ±2%, ±3%, and ±4% in the directions as explained by Mehl et al. [27,28] were applied to the structure, while allowing full relaxation of the ions to calculate the three independent elastic constants C_{11}, C_{12}, and C_{44}. We thus obtained the total minimum energies $E(V)$ at these strained volumes V, corresponding to each value of δ. These energies and strains were fit with the corresponding parabolic equation in the strains to obtain the elastic constants as detailed by Patil et al. [11].

For a crystal structure to be mechanically stable, the strain energy of the crystal should be positive for all values of strain δ. This imposes further restrictions on the elastic constants depending on the crystal structure. For cubic crystal structures such as those of zinc-blende, rocksalt, fluorite, or pyrite, the necessary conditions for mechanical stability are given by [29]

$$(C_{11}-C_{12})>0, (C_{11}+2C_{12})>0, C_{11}>0, C_{44}>0. \qquad (1)$$

3. Results and discussion

Table 1 shows the equilibrium lattice constants, elastic constants, bulk moduli and energy [30] per formula unit of fluorite phase MN_2 (M=Hf, Ta, W, Re, Os, Ir, Pt, Au). The elastic constants of HfN_2, TaN_2, and WN_2 violate the mechanical stability conditions given in Eq. (1) and hence are labeled unstable in Table 1. Table 1 also lists the previous theoretical calculations. Our calculations are in good agreement with previous investigations. Previous studies [7–10] have shown that fluorite phase OsN_2 and IrN_2 are super hard TMNs in period VI transition metals. Our calculations show that ReN_2 in fluorite phase is potentially super hard with B almost equal to that of OsN_2.

Table 2 shows the equilibrium lattice constants, elastic constants, bulk moduli and energy [30] per formula unit of pyrite phase MN_2 (M=Hf, Ta, W, Re, Os, Ir, Pt, Au). All pyrite phase TMNs of Table 2 obey the mechanical stability criterion given by Eq. (1) and hence are stable. It is interesting to see that HfN_2, TaN_2 and WN_2 which were unstable in fluorite phase are stabilized by pyrite phase. PtN_2 in pyrite phase was investigated before by Yu et al. [14] and the results obtained by them agree well with the present work [31]. The energy [30] per formula unit for all pyrite phases in Table 2 is less than that of the corresponding fluorite phase in Table 1, indicating their greater thermodynamic stability. WN_2 and ReN_2 in pyrite phase are found to have a high B of 334 GPa and 348 GPa respectively. These high values

of B for WN_2, ReN_2, OsN_2, IrN_2, and PtN_2 in both fluorite and pyrite phases make them potential candidates for hard coatings.

Table 3 shows the equilibrium lattice constants, elastic constants, bulk moduli and energy [30] per formula unit of zinc-blende and rocksalt phases of MN (M=Hf, Ta, W, Re, Os, Ir, Pt, Au). Only HfN, TaN, and IrN were found to be mechanically stable in zinc-blende phase with a B of 219 GPa, 274 GPa, and 289 GPa respectively. In rocksalt phase only HfN, TaN, PtN, and AuN were found to be mechanically stable with a B of 310 GPa, 380 GPa, 284 GPa and 217 GPa respectively. Owing to a high B, HfN and TaN in rocksalt phase are potential candidates for hard coatings. Very few experimental measurements of elastic constants of these stable HfN and TaN phases exist. For example, Ref. [32,33] and Ref. [34,35] report hardness and elastic moduli of HfN(001) and TaN(001) thin films respectively. Another experimental work [36] on nano-crystalline hexagonal Ta_2N yielded a high bulk modulus of 360 GPa. These measurements and our computations support further experimental investigation of elastic constants of bulk cubic nitride phases.

Bulk modulus is not the only mechanical quantity that determines the utility of a material for hard coatings. Hardness and toughness are important material properties also to be considered. It is known that measured hardness of the material correlates with the shear modulus (G) [37,38]. Toughness is influenced by the degree of plastic deformation (ductility) of the material under mechanical loading. For pure metals with the same lattice structure, ductility correlates with the B/G ratio [39]. As the TMNs investigated have a large component of metallic bonding (discussed later in the section detailing local density of states results), we have assumed, that the correlation of the ratio B/G with ductility holds good in the present case. Fig. 1 shows the ductility and hardness trends for the stable rocksalt, pyrite, and fluorite phases [40] of period VI TMNs. Shear

Table 2
Equilibrium lattice constant a, elastic constants C_{11}, C_{12} and C_{44}, bulk modulus B and energy [30] E per formula unit for pyrite phase of period VI transition metal nitrides

	a (Å)	C_{11} (GPa)	C_{12} (GPa)	C_{44} (GPa)	B (GPa)	E (eV)
HfN_2	5.029	305	222	64	250	−31.87
TaN_2	5.005	322	224	60	256	−31.79
WN_2	4.928	497	253	52	334	−31.75
ReN_2	4.880	521	261	80	348	−30.36
OsN_2	4.839 (4.925[a])	616 (523[a])	266 (213[a])	104 (107[a])	383 (316[a])	−28.68
IrN_2	4.781	804	147	79	366	−27.14
PtN_2	4.792	845 (824[b])	101 (117[b])	160 (152[b])	349 (352[b])	−24.69
AuN_2	5.005	453	343	61	380	−19.29

Refs. [10,14] are previous *ab initio* investigations.
  [a] Ref. [10].
  [b] Ref. [14].

Table 1
Equilibrium lattice constant a, elastic constants C_{11}, C_{12} and C_{44}, bulk modulus B and energy [30] E per formula unit for fluorite phase of period VI transition metal nitrides

	a (Å)	C_{11} (GPa)	C_{12} (GPa)	C_{44} (GPa)	B (GPa)	E (eV)
HfN_2	5.068	Unstable	Unstable	Unstable	251.1	Unstable
TaN_2	4.930	Unstable	Unstable	Unstable	323.8	Unstable
WN_2	4.855	Unstable	Unstable	Unstable	359.8	Unstable
ReN_2	4.820	426.0	345.3	36.0	372.2	−30.18
OsN_2	4.794 (4.781[a])	496.0 (544.5[a])	313.2 (309.8[a])	96.1 (103.9[a])	374.1 (388.0[a])	−28.36
IrN_2	4.815 (4.801[b])	459.7 (464.0[b])	306.9 (339.0[b])	128.8 (124.0[b])	357.8 (381.0[b])	−25.67
PtN_2	4.886 (4.866[b])	500.5 (532.0[b])	199.2 (208.0[b])	112.5 (122.0[b])	299.7 (316.0[b])	−21.99
AuN_2	5.068 (5.035[b])	349.9 (371.0[b])	179.2 (183.0[b])	71.0 (71.0[b])	236.1 (246.0[b])	−16.50

Refs. [9,10] are previous *ab initio* investigations.
  [a] Ref. [10].
  [b] Ref. [9].

Table 3
Equilibrium lattice constant a, elastic constants C_{11}, C_{12} and C_{44}, bulk modulus B and energy [30] E per formula unit for zinc-blende (zb) and rocksalt (rs) phases of period VI transition metal nitrides

|		a (Å)	C_{11} (GPa)	C_{12} (GPa)	C_{44} (GPa)	B (GPa)	E (eV)
HfN	(zb)	4.796	326.1	166.5	107.7	219.7	−23.25
	(rs)	4.436	704.9	111.8	131.0	309.5	−24.11
TaN	(zb)	4.659	314.9	258.8	13.0	274.2	−23.82
	(rs)	4.326	826.9	155.9	73.4	379.6	−24.47
WN	(zb)	4.584	Unstable	Unstable	Unstable	308.3	Unstable
	(rs)	4.281	Unstable	Unstable	Unstable	407.0	Unstable
ReN	(zb)	4.543	Unstable	Unstable	Unstable	325.1	Unstable
	(rs)	4.276	Unstable	Unstable	Unstable	403.4	Unstable
OsN	(zb)	4.527	Unstable	Unstable	Unstable	327.2	Unstable
	(rs)	4.287	Unstable	Unstable	Unstable	381.4	Unstable
IrN	(zb)	4.573	316.2	275.8	55.8	289.3	−17.99
	(rs)	4.328	Unstable	Unstable	Unstable	346.0	Unstable
PtN	(zb)	4.699	Unstable	Unstable	Unstable	230.3	Unstable
	(rs)	4.407	355.0	248.0	36.0	284	−24.10
AuN	(zb)	4.870	Unstable	Unstable	Unstable	161.1	Unstable
	(rs)	4.5648	312.5	169.4	28.8	217.1	−10.31
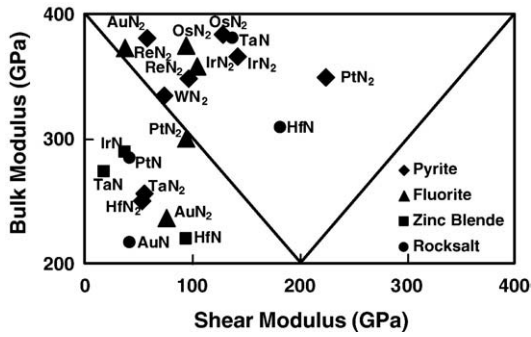
Fig. 1. Bulk (*B*) and shear (*G*) moduli of stable period VI transition metal nitrides in zinc-blende, rocksalt, fluorite and pyrite phases.

moduli have been calculated (in Fig. 1) using the limits provided by Hashin and Shtrikman [41,42]. For designing hard coatings for some cutting tool applications, the material should be hard as well as tough to resist erosion and wear [43]. These are two conflicting material properties in design of hard coatings for cutting tools as $B/G \ll 1$ corresponds to increasing hardness and $B/G \gg 1$ correlates to increasing ductility. Optimum materials fall into a central triangle bounded by regions of high hardness and ductility as shown in Fig. 1 It can be seen that MN_2 (M=Re, Ir, Os, Pt) in pyrite phase, OsN_2 and IrN_2 in fluorite phase and HfN and TaN in rocksalt phase obey this criterion
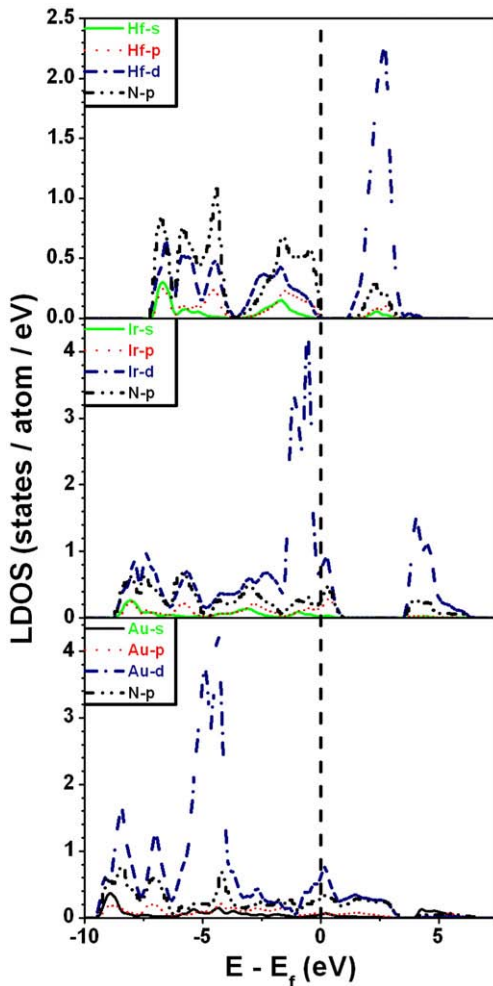
and are hence suited for synthesizing hard coatings. A consistency check for this analysis is realized from the fact that TaN is already in use in such applications.

Local density of states (LDOS) was obtained for all the phases of TMNs investigated. Only few LDOS plots are displayed here for brevity. Except for HfN_2 and PtN_2 in pyrite phase all other TMNs investigated were found to be metallic, with no energy band gap at the Fermi energy, in the LDOS. Fig. 2 shows the LDOS for pyrite phase HfN_2, IrN_2, and AuN_2. The trend in *B* can be related to LDOS. The hybridization of the various metal (M) and nitrogen (N) p electronic states is shown by the overlapping peaks in plots of their respective densities. Fig. 2 shows two interesting features: (i) The hybridization peak of M d-orbital coincident with the N p-orbital. All other energy levels (metal s, p and nitrogen s orbital) do not contribute much to this bond. This nature of bonding is found to be universal for all the phases studied. (ii) The hybridization at Fermi level is strong for pyrite IrN_2 and AuN_2 when compared to pyrite HfN_2. This could be the reason for higher *B* of IrN_2 and AuN_2. Fig. 3 shows the LDOS for the fluorite and pyrite phases of WN_2. A very high density of states at Fermi level exists for fluorite phase of WN_2 which could lead to the instability of the electronic structure resulting in structural distortions [15,16]. But the crystal structure in pyrite phase is not prone to this instability and is therefore mechanically stable. HfN_2 and TaN_2 in fluorite phase showed the same trend of high density of states at Fermi level making them unstable but were stabilized in pyrite phase by the shift in the density of states peak away from the Fermi energy.

It has been shown in earlier studies [3,4] that mechanical properties may be related to valence electron density (VED) per unit cell. In our study we found some similar correlations. For fluorite and pyrite phases, VED increases in steps of unity from 14 for HfN_2 to 20 for PtN_2 as each extra electron is added to the d-orbital. In case of both fluorite and pyrite phases, *B* increases from HfN_2 to OsN_2 and decreases from OsN_2 to PtN_2. *B* peaks at OsN_2 with a VED of 18. It may be speculated that 18 being a number associated with the valence shell configuration of the noble elements, which are chemically very
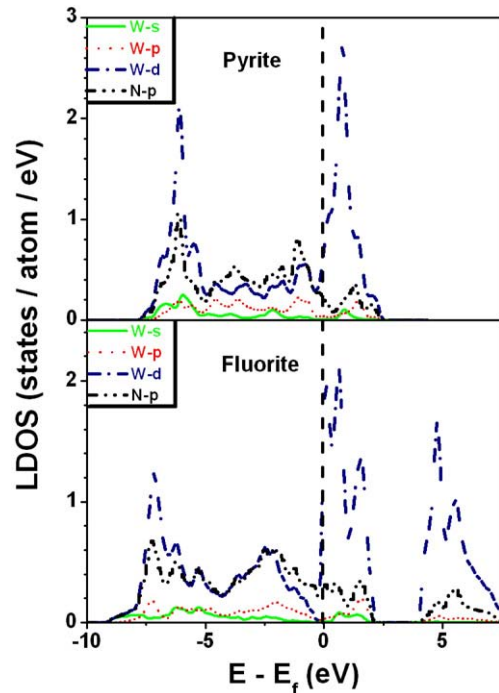

Fig. 2. Local density of states (LDOS) for pyrite phases of HfN_2, IrN_2, and AuN_2. The Fermi energy is set to zero as shown by the dashed vertical line. The density of the N s-states is not shown since it is vanishingly small in the energy range shown.

Fig. 3. Local density of states (LDOS) for pyrite phases of WN_2, in pyrite and fluorite phases. The Fermi energy is set to zero as shown by the dashed vertical line. The density of the N s-states is not shown since it is vanishingly small in the energy range shown. The total density of states at the Fermi energy is much larger in the unstable fluorite phase compared to the stable pyrite phase.

stable, may have a causal relationship with the peaking of *B* values. These findings are qualitatively similar to those obtained with *ab initio* computations by Jhi et al. [3] concluding that the family of transition metal carbo-nitrides had a peak shear modulus at a VED of 8.4/cell. Holleck [4] also showed that at a VED of 8.4 some metal nitrides and carbides achieve maximum hardness.

4. Conclusion

In summary, we have performed an exhaustive study of cubic phases of period VI transition metal nitrides. Our investigation predicts that ReN_2 in fluorite and pyrite phases and WN_2 in pyrite phase should be mechanically stable with a high *B*. We further tested the suitability in hard coating applications of this class of cubic transition metal nitrides (zinc-blende, rocksalt, fluorite, and pyrite phases). The high *B* is attributed to metal d and nitrogen p-orbital hybridization. The mechanical instability of the unstable phases is linked to high DOS at Fermi level. The bulk modulus for both pyrite and fluorite phases has a peak at a valence electron density of 18. We hope that the present calculations would lead to the synthesis of hard WN_2 and ReN_2 and motivate the research of these crystal structures in the hard coatings industry.

Just before publication we became aware of recent work in synthesis and prediction of hard nitrides [44–46].

Acknowledgements

References

[1] L.E. Toth, Transition Metal Carbides and Nitrides, Academic, New York, 1971.
[2] H. Pierson, Handbook of Refractory Carbides and Nitrides: Properties, Characteristics and Applications, Noyes Publications, Westwood, NJ, 1996.
[3] S.-H. Jhi, J. Ihm, S.G. Louie, M.L. Cohen, Nature (London) 399 (1999) 132.
[4] H. Holleck, J. Vac. Sci. Technol., A, Vac. Surf. Films 4 (1986) 6.
[5] S. Krishnamurthy, M. Montalti, M.G. Wardle, M.J. Shaw, P.R. Briddon, K. Svensson, M.R.C. Hunt, L. Siller, Phys. Rev., B 70 (2004) 045414.
[6] E. Gregoryanz, C. Sanloup, M. Somayazulu, J. Bardo, G. Fiquet, H.-K. Mao, R. Hemley, Nat. Mater. 3 (2004) 294.
[7] J.C. Crowhurst, A.F. Goncharov, B. Sadigh, C.L. Evans, P.G. Morrall, J.L. Ferreira, A.J. Nelson, Science 311 (2006) 1275.
[8] A.F. Young, C. Sanloup, E. Gregoryanz, S. Scandolo, R.J. Hemley, H.K. Mao, Phys. Rev. Lett. 96 (2006) 155501.
[9] R. Yu, X.F. Zhang, Phys. Rev., B 72 (2005) 054103.
[10] C.Z. Fan, S.Y. Zeng, L.X. Li, Z.J. Zhan, R.P. Liu, W.K. Wang, P. Zhang, Y.G. Yao, Phys. Rev., B 74 (2006) 125118.
[11] S.K.R. Patil, S.V. Khare, B.R. Tuttle, J.K. Bording, S. Kodambaka, Phys. Rev., B 73 (2006) 104118.
[12] C.Z. Fan, L.L. Sun, Y.X. Wang, Z.J. Wei, R.P. Liu, S.Y. Zeng, W.K. Wang, Chin. Phys. Lett. 22 (2005) 2637.
[13] R. Yu, X.F. Zhang, Appl. Phys. Lett. 86 (2005) 121913.
[14] R. Yu, Q. Zhan, X.F. Zhang, Appl. Phys. Lett. 88 (2006) 051913.
[15] Y.X. Wang, M. Arai, T. Sasaki, Appl. Phys. Lett. 90 (2007) 061922.
[16] J.A. Montoya, A.D. Hernandez, C. Sanloup, E. Gregoryanz, S. Scandolo, Appl. Phys. Lett. 90 (2007) 011909.
[17] P. Hohenberg, W. Kohn, Phys. Rev., B 136 (1964) 864;
    W. Kohn, L.J. Sham, Phys. Rev., A 140 (1965) 1133.
[18] G. Kresse, J. Hafner, Phys. Rev., B 47 (1993) 558.
[19] G. Kresse, Thesis, Technische Universiät Wien 1993.
[20] G. Kresse, J. Furthmüller, Comput. Mater. Sci. 6 (1996) 15.
[21] G. Kresse, J. Furthmüller, Phys. Rev., B 54 (1996) 11169.
[22] D. Vanderbilt, Phys. Rev., B 41 (1990) 7892.
[23] G. Kresse, J. Hafner, J. Phys.: Condens. Matter 6 (1994) 8245.
[24] H.J. Monkhorst, J.D. Pack, Phys. Rev., B 13 (1976) 5188.
[25] P.E. Blöchl, Phys. Rev., B 50 (1994) 17953.
[26] D.M. Teter, G.V. Gibbs, M.B. Boisen Jr., D.C. Allan, M.P. Teter, Phys. Rev., B 52 (1995) 8064.
[27] M.J. Mehl, J.E. Osburn, D.A. Papaconstantopoulos, B.M. Klein, Phys. Rev., B 41 (1990) 10311.
[28] M.J. Mehl, J.E. Osburn, D.A. Papaconstantopoulos, B.M. Klein, Phys. Rev., B 42 (1990) 5362.
[29] D.C. Wallace, Thermodynamics of Crystals, Wiley, New York, 1972 Chap. 1.
[30] These energies give reliable trends for relative stabilities of different phases. However, these absolute theoretical values cannot be directly compared with experimentally measured cohesive energies.
[31] The difference between our results and results of Fan [10,12] et al. is because of the differences in the methods of computations. Fan et al. used general gradient approximation (GGA) and the present work uses LDA. It is well known that LDA over estimates the bulk modulus slightly, underestimates the lattice constant and conversely GGA under estimates the bulk modulus and over estimates the lattice constant.
[32] H.-S. Seo, T.-Y. Lee, J.G. Wen, I. Petrov, J.E. Greene, D. Gall, J. Appl. Phys. 96 (2004) 878.
[33] H.-S. Seo, T.-Y. Lee, I. Petrov, J.E. Greene, D. Gall, J. Appl. Phys. 97 (2005) 083521.
[34] C.-S. Shin, D. Gall, P. Desjardins, A. Vailionis, H. Kim, I. Petrov, J.E. Greene, M. Oden, Appl. Phys. Lett. 75 (1999) 3808.
[35] C.-S. Shin, D. Gall, Y.-W. Kim, P. Desjardins, I. Petrov, J.E. Greene, M. Oden, L. Hultman, J. Appl. Phys. 90 (2001) 2879.
[36] W.W. Lei, D. Liu, X.F. Li, J. Zhang, Q. Zhou, J.Z. Hu, Q.L. Cui, G.T. Zou, J. Phys.: Condens. Matter 19 (2007) 425233.
[37] A. Kelly, N.H. Macmillan, Strong Solids, Third edition. Clarendon, Oxford, 1986.
[38] D.M. Teter, Mater. Res. Soc. Bull 23 (1998) 22.
[39] S.F. Pugh, Philos. Mag. 45 (1954) 823.
[40] None of the stable zinc-blende phases were found to be suitable for hard coating applications.
[41] Z. Hashin, S. Shtrikman, J. Mech. Phys. Solids 10 (1962) 335.
[42] Z. Hashin, S. Shtrikman, J. Mech. Phys. Solids 10 (1962) 343.
[43] L.R. Zhao, K. Chen, Q. Yang, J.R. Rodgers, S.H. Chiou, Surf. Coat. Technol. 200 (2005) 1595.
[44] A. Simunek, Phys. Rev., B 75 (2007) 172108.
[45] M.G. Moreno-Armenta, J. Diaz, A. Martinez-Ruiz, G. Soto, J. Phys. Chem. Solids 68 (2007) 1989.
[46] D. Aberg, B. Sadigh, J.C. Crowhurst, A.F. Goncharov, Phys. Rev. Lett. 100 (2008) 095501.